Electronic Supporting Information

Efficient photoelectrocatalytic radical dichlorination of alkenes via synergism with Mn

Yuanjun He,[a,b,†] Qiaozhen Li,[b,c,†] Daojian Tang,[b,c] Ruiying Li[a], Jian Liu,[a] Yuchao Zhang,[b,c,*] and Jincai Zhao[b,c]

[a] State Key Laboratory of Heavy Oil Processing, College of Science, China University of Petroleum, Beijing, 102249, P. R. China.
[b] Beijing National Laboratory for Molecular Sciences, Institute of Chemistry, Chinese Academy of Sciences, Beijing 100190, P. R. China. E-mail: yczhang@iccas.ac.cn.
[c] University of Chinese Academy of Sciences, Beijing 100049, P. R. China.
[†] These authors contributed equally.

Table of contents

1. Materials and synthesis of photoanodes:

Fluorine-doped tin oxide substrates (FTO, 2.2 mm) were purchased from Nippon Plate Glass Co., Ltd. Iron (III) chloride anhydrous ($FeCl_3$) (98%), titanium (IV) butoxide (97%) and manganese chloridewas (98%) purchased from Alfa Aesar. Ammonium oxalate monohydrate (98%) was purchased from Macklin. Sodium tungstate dihydrate (97%), sodium chloride (99.9%), styrene (99%), tetraethylammonium tetrafluoroborate (Net_4BF_4, 98%) and acetonitrile (99.9%, extra dry with molecular sieves, Water ≤ 50 ppm) were purchased from Innochem. Concentrated hydrochloric acid (HCl, 37 wt%) was purchased from Sinopharm. All chemicals were used as received without further purification.

Photoanodes preparation:

Three photoanodes were all prepared on fluorine-doped tin oxide substrates (FTO). FTO needed to be cleaned with acetone, ethanol and deionized water by ultrasonication for 30 min prior to preparation.

Preparation of TiO_2 Photoanodes:

The TiO_2 photoanode was synthesized using the hydrothermal method reported previously.[1]

The 15 mL concentrated HCl (37 wt %) was added to 25 mL ultra-pure water slowly with stirring. After sufficient stirring for 15 min, 1 mL of titanium (IV) butoxide was slowly added dropwise and continued stirring for 30 min. 7.2 mL of mixed precursor solution and the processed FTO were transferred to the 20 mL Teflon-lined autoclave and heated at 150 ℃ for 6 h. Getting TiO_2 nanowires.

The obtained TiO_2 was rinsed with ultra-pure water, and placed in the muffle furnace to anneal for 1.5 h at 450 ℃ under air atmosphere for to improve the crystallinity of the TiO_2 nanorods and enhance the contact with the FTO substrate.

Preparation of WO_3 Photoanodes:

WO_3 was synthesized using the method reported.[2]

Sputtering a 1 nm tungsten metal layer onto the conductive side of FTO and placed in a muffle furnace and annealed for 2 h at 500 °C in an air atmosphere.

0.206 g of $Na_2WO_4•2H_2O$ was dissolved into 30 mL of ultra-pure water, with string 10 min. And 1.5 mL of concentrated HCl (37 wt%) was followed added, stirring for 30 min until the yellow precipitate appeared. Quickly added 0.8 g $(NH_4)_2C_2O_4•H_2O$ and continue stirring until the solution became clear. Then the solution was diluted to 70 mL with ultra-pure water. 8 mL of mixed precursor solution and the processed FTO were transferred to the 25 mL Teflon-lined autoclave and heated at 160 ℃ for 6 h. Getting WO_3 nanosheet.

The obtained WO_3 was rinsed with ultra-pure water, then placed in the muffle furnace to anneal for 2 h at 500 ℃ under air atmosphere and cooled to room temperature.

Preparation of α-Fe_2O_3 Photoanodes:

The α-Fe_2O_3 photoanode was also synthesized using the hydrothermal method reported previously.[3]

The 100 μL concentrated HCl (37 wt %) was added to 100 mL ultra-pure water. The solution was added in 0.85 g $NaNO_3$, 2.43 g $FeCl_3$. The solution was sealed and then stirred magnetically for 10 min to dissolve all the solids. 7.5 mL of mixed precursor solution and the processed FTO were transferred to the 20 mL Teflon-lined autoclave and heated at 95 ℃ for 4 h, getting FeOOH nanowires.

The obtained light yellow FeOOH/FTO was rinsed with ultra-pure water, then placed in the muffle furnace to anneal for 2 h at 550 ℃ under air atmosphere and rose to 750 ℃ for 15 min, finally cooled to room temperature to get the α-Fe_2O_3.

2. Experimental methods

2.1 Physical characterization:

X-ray diffraction (XRD) patterns were collected on an X-ray diffractometer instrument (Empyrean, PANalytical) with 5°/min over a 2θ value range from 20° to 80°. The surface morphology of samples was characterized by field emission scanning electron microscope (FESEM, Hitachi, 7500F). Ultraviolet-visible diffuse reflectance spectrums (UV-vis DRS) was carried out with a Hitachi U-3900 spectrometer. X-ray photoelectron spectroscopy (XPS) was conducted on the Thermo Scientific ESCALab 250Xi spectrometer equipped with 300 W Al Kα radiation. The hydrocarbon C 1s line at 284.8 eV from adventitious carbon is used for calibration.

2.2 PEC measurement:

PEC measurements were performed in a three-electrode electrochemical cell controlled by an electrochemical workstation (CHI1040E), with Pt wire as the counter electrode and Ag/AgCl as the reference electrode. Under the H-type cell, nafion proton exchange membrane was used to separate the photoanode from the cathode chamber. Unless specifically labeled, the PEC experiments were conducted in a 10 mL solution. The test Solution was the 50% H_2O and 50% CH_3CN (V%) mixed solution with 0.1 M NaCl (pH = 6.4) as the electrolyte and the chlorine source. Under the undivided cell, experiments were conducted in a 4 mL solution of 2% H_2O and 98% CH_3CN (V %) mixed solution with 0.1 M Net_4BF_4 as the electrolyte and the 4 eq HCl as chlorine source. The reactions products under the simulated sunlight (AM 1.5G, 100 mW/cm^2) obtained by a Xenon lamp. The PEC experiments were performed with magnetic stirring at 900 rpm, and a water recycling system was used to prevent the solution from heating up during reactions.

2.3 Electron paramagnetic resonance (EPR) measurements:

5,5-dimethyl-1-pyrroline N-oxide (DMPO) and N-tert-butyl-α-phenylnitrone (PBN) were used as the spin-trap reagent to capture potential radicals generated during the reaction process. The measurements were conducted in an open-type cell, which was based on the previously reported method.[4]

During the PEC process, use a pipette to add 20 μL DMPO/PBN into the solution on the surface of the photoanode. It was significant to note that the tip of the pipette needed to be closed to the photoanode, ensuring that formed radical species can be

captured as much as possible. Subsequently, the solution on the photoanode surface was immediately collected for EPR measurements.

2.4 Product analysis:

All products resulting from PEC reactions were subjected to analysis using GC-MS or NMR techniques to validate their identity. The GC-MS analyses were conducted utilizing an Agilent instrument equipped with an HP-5ms GC column and an electron ionization ion source, with a solvent delay time of 3 min. The chlorination products of toluene were quantified by GC. Measurements were run on an Agilent GC instrument with a DB-VRX GC column and FID detector. The chlorination products of styrene (**1a−3a**) were quantified by high-performance liquid chromatography (HPLC) equipped with a DAD detector. The chromatographic column was a C18 column with a mobile phase ratio of 30% H_2O, 70% CH_3CN (V%) and a detection wavelength of 225 nm. In the substrate development experiments (**1-18**), the chlorinated products were extracted with ethyl acetate and concentrated by spinning instruments, and then quantified by NMR with 1,3,5-trimethoxybenzene as the internal standard substrate.

The value of chlorination product selectivity and Faradaic efficiency (FE) are calculated by the following equations:

$$Selectivity = \frac{contennt\ of\ corresponding\ product}{consumption\ of\ reactant} \times 100\%$$;

$$Faradaic\ efficiency(FE) = \frac{2nF}{Q} \times 100\%$$ (where n was the number of electrons transferred by the chlorination reaction, F is the Faraday constant, and Q denoted the quantity of electric charge of reaction process.);

$$Yield\ rate = \frac{the\ productivity\ of\ products}{t \times A}$$ (where t was the reaction time, and A was the area of photoanode (2 cm^{-2})).

3. Other supporting figures and tables

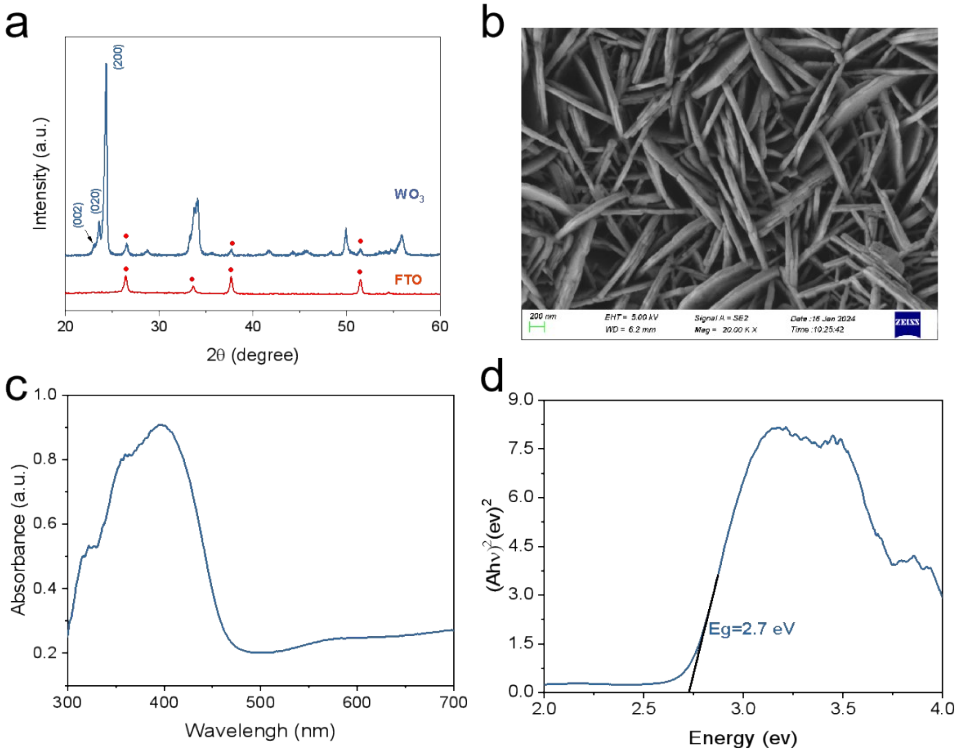

Figure S1. Structural characterizations of WO_3. (a) XRD patterns, (b) SEM image of an WO_3 photoanode. (c) UV-vis spectrum and (d) the corresponding Tauc plot of an WO_3 photoanodes.

The XRD pattern (Figure S1a) of the as-prepared photoanode was well matched to the monoclinic WO_3 (PDF# 43-1035). The diffraction peaks at $2\theta = 23.1°$, 23.6° and 24.4° were assigned to the (002), (020), and (200) peaks respectively.[5, 6] The SEM image (Figure S1b) indicated that the as-prepared WO_3 film consisted of numerous nanoflakes. The UV-vis DRS (Figure S1c) evaluated the light absorption of as-prepared photoanode, and the corresponding Tauc plot (Figure S1d) was obtained with an optical band gap of 2.7 eV. These results illustrated the successful preparation of WO_3 photoanode.[7]

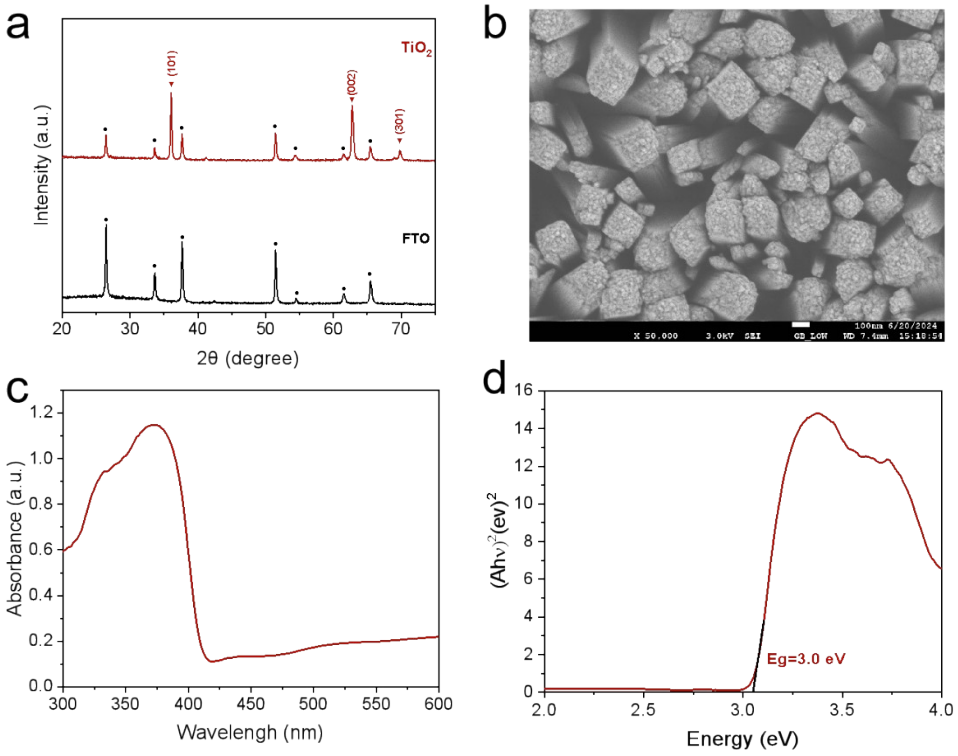

Figure S2. Structural characterizations of TiO_2. (a) XRD patterns, (b) SEM image of an TiO_2 photoanode. (c) UV-vis spectrum and (d) the corresponding Tauc plot of an TiO_2 photoanodes.

The XRD (Figure S2a) confirmed that the as-prepared photoanode exhibited a strong resemblance to the rutile phase of TiO_2 (PDF# 21-1276).[8] The characteristic diffraction peaks observed at 2θ=36.5°, 63.3°, and 70.3° respectively corresponded to the (101), (002), and (301) crystal plane. The SEM imaging (Figure S2b) revealed the presence of numerous nanorod within the TiO_2 film. The UV-vis DRS (Figure S2c) assessed the light absorption properties of the photoanode. The resulting Tauc plot (Figure S2d) analysis yielded an optical band gap value of 3.0 eV. These findings validated the effective preparation of the TiO_2 photoanode.[9, 10]

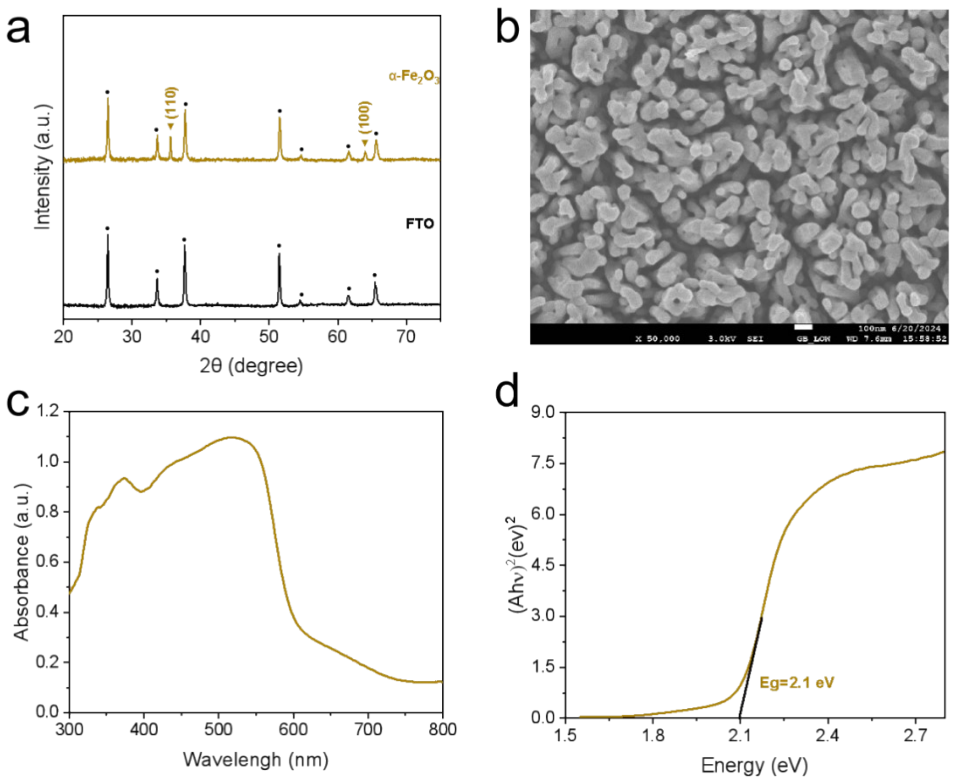

Figure S3. Structural characterizations of α-Fe_2O_3. (a) XRD patterns, (b) SEM image of an α-Fe_2O_3 photoanode. (e) UV-vis spectrum and (f) the corresponding Tauc plot of an α-Fe_2O_3 photoanodes.

The XRD analysis (Figure S3a) revealed a high degree of correspondence with the α-Fe_2O_3, indexed as PDF# 33-0664, characterized by prominent peaks at 2θ angles of 35.6° and 64.0° attributed to the (110) and (100) plane.[3] The SEM micrograph (Figure S3b) depicted the film of nanorod. The UV-vis DRS (Figure S3c) showed the light absorption properties of the synthesized photoanode, resulting in a calculated optical bandgap of 2.1 eV (Figure S3d), substantiating the successful fabrication of the α-Fe_2O_3 photoelectrode.[4, 11]

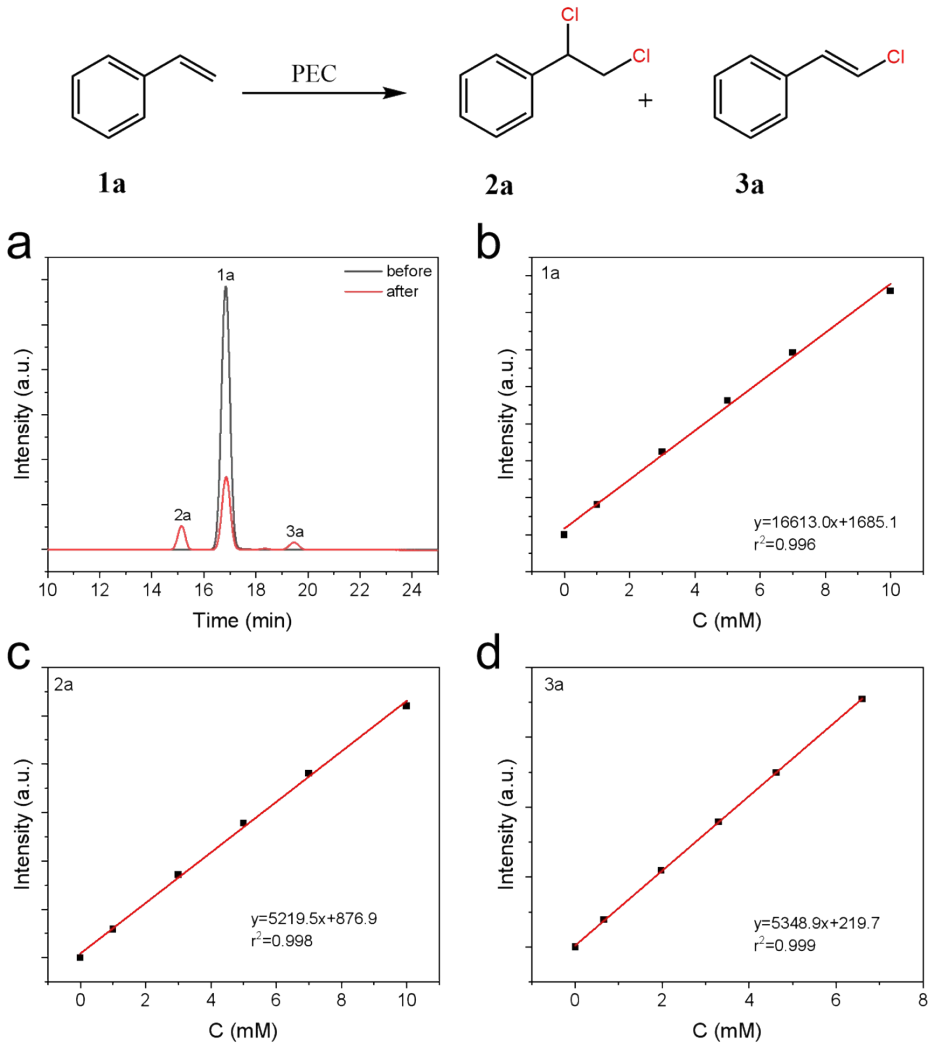

Figure S4. The quantification of alkene chlorination products. (a) HPLC spectra of styrene chlorination products. (b-d) The external standard curves of styrene and chlorination products. Measurements were run on an Agilent LC instrument with a C18 column and DAD detector. Detection wavelength was 225 nm and mobile phase ratio was 30% H_2O and 70% CH_3CN (V%).

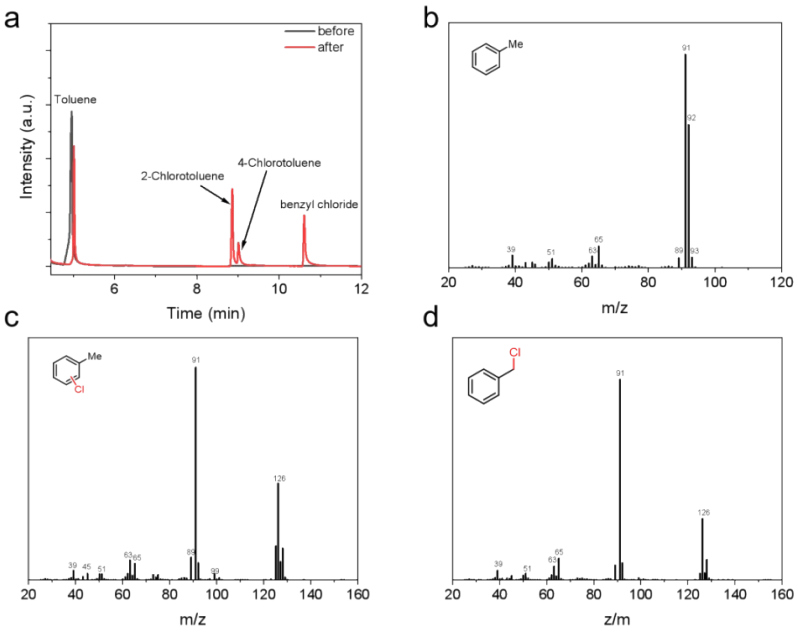

Figure S5. PEC chlorination experiment of toluene. (a) GC spectrum of the products. (b−d) The MS spectra of chlorination products. *The reaction performed under the undivided type cell with 4 mL solution (2% H_2O, 98% CH_3CN (V%)), including 0.1 M NaCl and 0.1 mmol toluene. The electrolysis potential was 1.0 V vs. Ag/AgCl. The electrolyte was bubbled with Ar gas flow for 10 min to remove air. The reaction was carried out for 2 h.

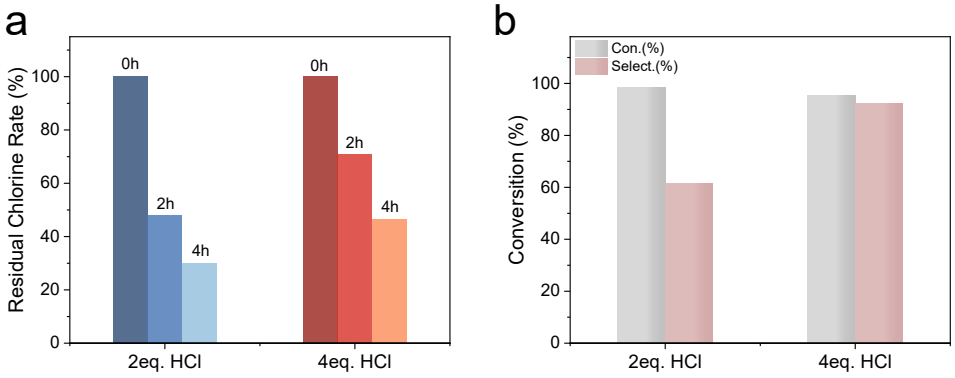

Figure S6. (a) The residual chlorine rate of Cl^- after 2 hours and 4 hours of reaction under different HCl concentration conditions using High Performance Ion Chromatography (HPIC). (b) The conversion rate of styrene and the selectivity for dichlorinated products after 4 hours of reaction under different hydrochloric acid concentration conditions.

We measured the chloride ion (Cl^-) concentration before and after the reaction using High Performance Ion Chromatography (HPIC) (Figure S6a). The results confirmed that under the condition of 2 eq. of HCl, a small amount of Cl^- would no longer be oxidized during later stages of the reaction. Figure S6b showed that under the condition of 2 eq. of HCl, the selectivity of the dichlorinated product decreased. We speculated that the low chloride ion concentration in the later reaction stage led to increased competitive adsorption of styrene on the electrode surface, which resulted in its direct oxidation and the formation of byproducts. However, under the condition of 4 eq. of HCl, after 4 hours of reaction, the consumption of Cl^- matched the theoretical value, and the selectivity of the dichlorinated product remained at a high level. Therefore, we believed that under the condition of 4 eq. of HCl, all the active chlorine generated was used for the dichlorination reaction. While byproducts such as Cl_2 might form during the reaction, but very minimal. The excess chloride ions were introduced specifically to prevent a drop in chloride concentration in the later phase of the reaction, thereby avoiding competitive adsorption of styrene and the consequent decline in dichlorinated product selectivity.

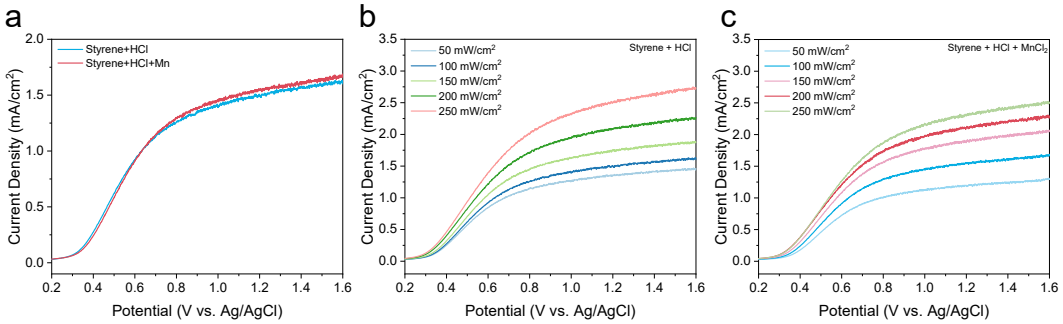

Figure S7. (a) The Linear Sweep Voltammetry (LSV) curves under simulated sunlight before and after the addition of Mn^{2+}. The LSV curves of dichlorination performance under different light intensities before (b) and after (c) the addition of Mn^{2+}.

The Linear Sweep Voltammetry (LSV) curves under different light intensities (Figure S7b, c) were found that the photocurrent gradually increased with the increase in light intensity. Additionally, the addition of $MnCl_2$ did not affect the photocurrent. (Figure S7a)

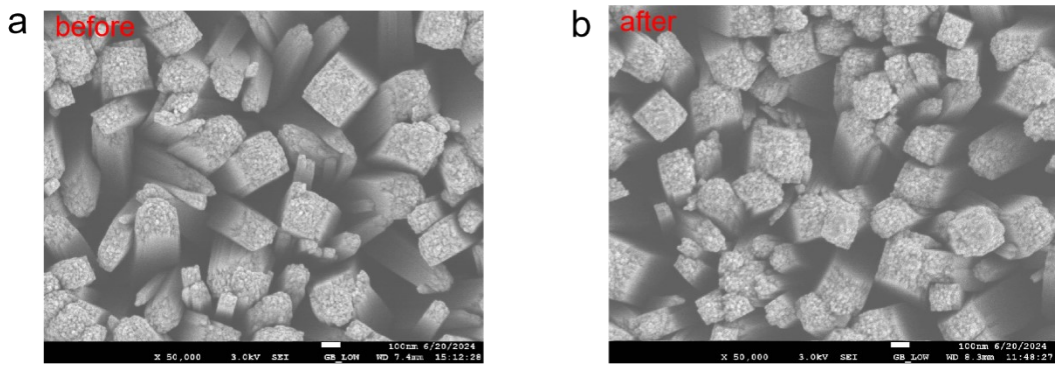

Figure S8. The SEM imagines of TiO_2 (a) before and (b) after the reaction.

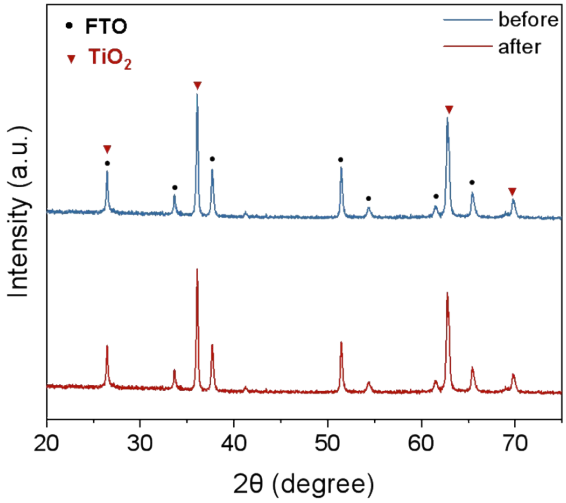

Figure S9. The XRD patterns of TiO_2 before and after the reactions.

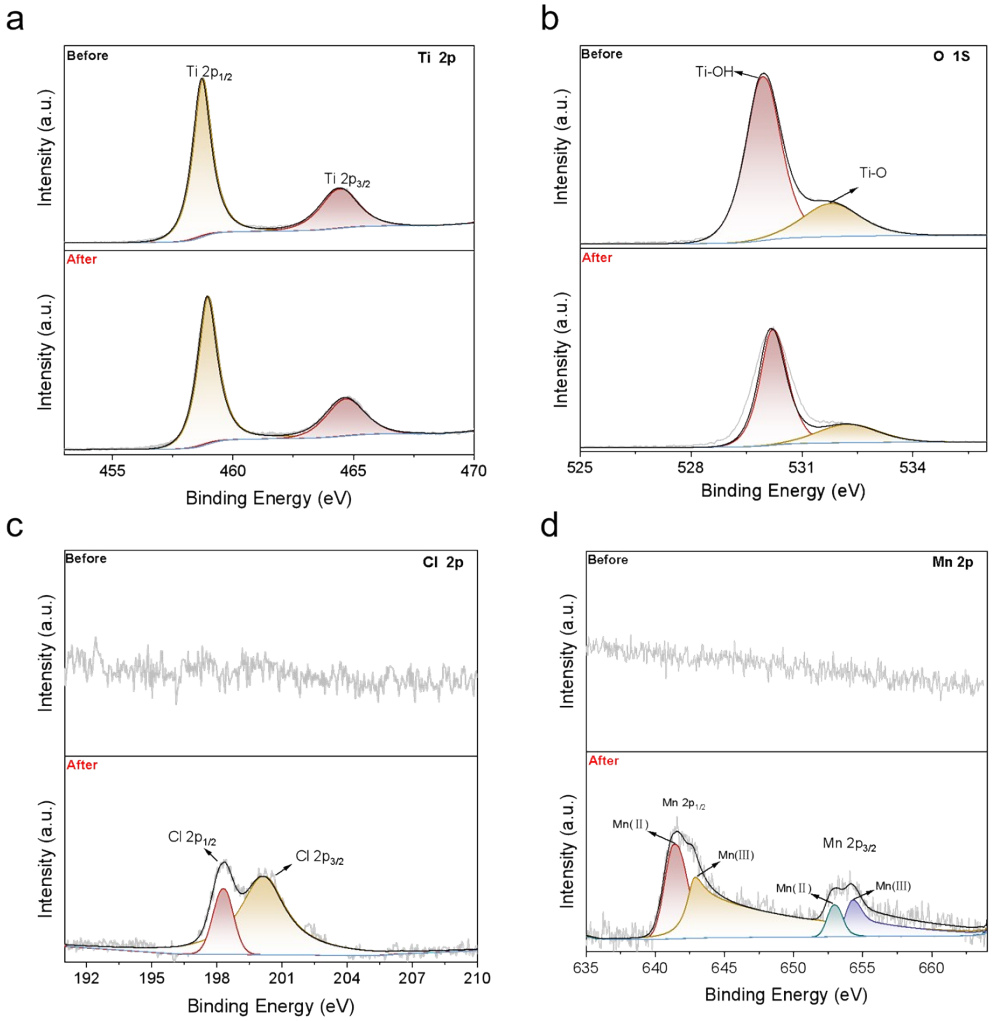

Figure S10. XPS characterizations of TiO_2 before and after the reaction. (a) XPS spectra of the Ti 2p core level and (b) the O 1s core level (c) the Cl 2p core level and (d) the Mn 2p core level.

The peaks centered at binding energies of 458.8 and 464.6 eV were attributed to Ti $2p_{3/2}$ and $2p_{1/2}$ (Figure S8a).[8, 9] And the O 1s peaks were corresponded to 531.7 and 530.1 eV. The O 1s spectra center at 531.7 and 530.1 eV were correspond to adsorbed oxygen (Ti-OH) and lattice oxygen (Ti-O) (Figure S8b).[12] The XPS spectra and the peak position were consistent with the typical values for TiO_2. Meanwhile, there was no notable shift in peak position and binding energy of Ti 2p after six consecutive cycles of reaction. The peaks of O 1s exhibited a slight shift to lower binding energy after the reaction because of the absorption of Mn^{2+} and Cl^{-}.[13]

The Cl 2p spectra (Figure S8c) were deconvoluted into Cl $2p_{3/2}$ and Cl $2p_{1/2}$ peaks, which are respectively centered 198.2 eV and 200.3 eV.[14, 15] The peaks centered at 652.88 and 641.68 eV corresponding to Mn $2p_{1/2}$ and Mn $2p_{3/2}$, respectively, matched the binding energy of Mn^{2+} signal (Figure S8d). Additionally, the additional peaks observed at 654.48 and 643.58 eV are associated with Mn^{3+}.[16, 17]

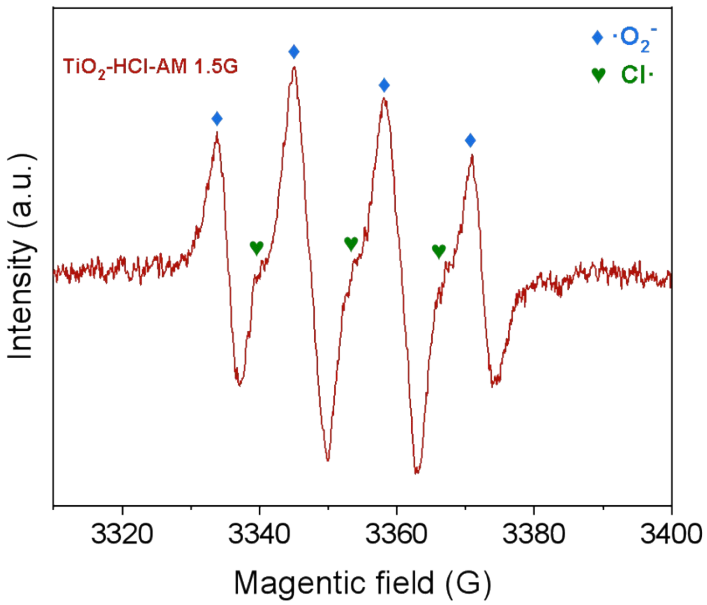

Figure S11. EPR spectra of the solution with Mn^{2+} obtained from an in-situ trapping method during PEC oxidation on TiO_2 over 3250 to 3450G magnetic field, using the addition of DMPO as radical capture reagent. *The reaction performed under the open-type cell with 5 mL solution (2% H_2O, 98% CH_3CN (V%)) for 120 s, including 0.1 M $LiClO_4$, 0.1 mmol HCl, 10 μmol $MnCl_2$ and 20 mM DMPO as the radical capture reagent. The electrolysis potential was 1.0 V vs. Ag/AgCl.

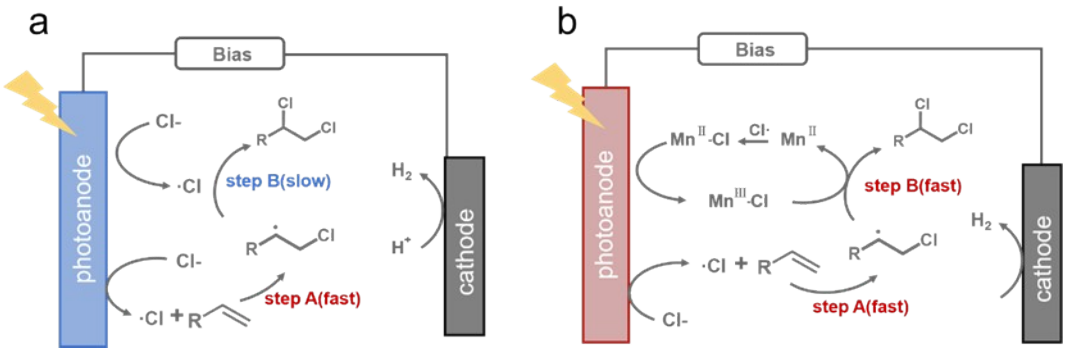

Figure S12. The comparative mechanism of the reaction pathways with (b) and without (a) Mn^{2+}.

Table S1. Exploration of activities of alkene chlorination on TiO_2 photoanodes under different chlorine sources and various electrolytes.

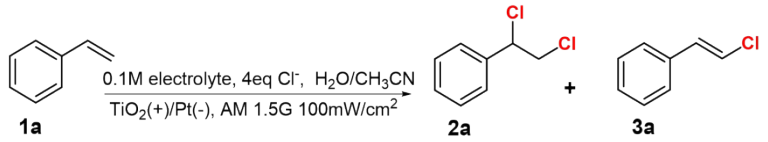

Entry	Cl sorce	acid.	Electrolyte	Yield (%)	FE (%)
1	HCl (4 eq)		NEt_4BF_4	70	72
2	HCl (4 eq)		NBu_4BF_4	47	49
3	HCl (4 eq)		$LiClO_4$	40	51
4	HCl (4 eq)		NMe_4BF_4	47	45
5	HCl (4 eq)		NEt_4BF_4	19	26
6	NaCl (4 eq)	--	NEt_4BF_4	55	52
7	NaCl (4 eq)	HOAc	NEt_4BF_4	36	38
8	LiCl (4 eq)	HOAc	NEt_4BF_4	38	40
9	$MgCl_2$ (2 eq)	HOAc	NEt_4BF_4	37	37

*The reaction was performed in the undivided cell with 4 mL solution (2% H_2O, 98% CH_3CN (V%)), including 0.1 M electrolyte, 0.1 mmol styrene and 4 eq Cl^-. The electrolyte was bubbled with Ar gas flow for 10 min to remove air. The reaction was carried out for 2 h. The Yields and FEs were determined with HPLC.

Table S2. Exploration of activities of alkene chlorination on TiO_2 photoanodes under varying water contents and applied potentials.

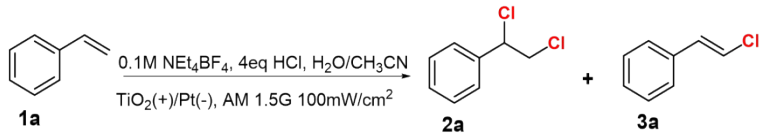

Entry	Potential(V)	H_2O content(V%)	Select. (%)	FE (%)
1	1.0	1%	53	70
2	1.0	2%	75	72
3	1.0	4%	56	67
4	1.0	6%	42	51
5	1.0	8%	31	43
6	1.2	2%	57	64
7	0.8	2%	73	76
8	0.6	2%	41	40

*The reaction was performed in the undivided cell with 4 mL solution (H_2O and CH_3CN (V%)), including 0.1 M NEt_4BF_4, 0.1 mmol styrene and 4 eq HCl. The electrolyte was bubbled with Ar gas flow for 10 min to remove air. The reaction was carried out for 2 h. The Yields and FEs were determined with HPLC.

1,2-dichlorostyrene

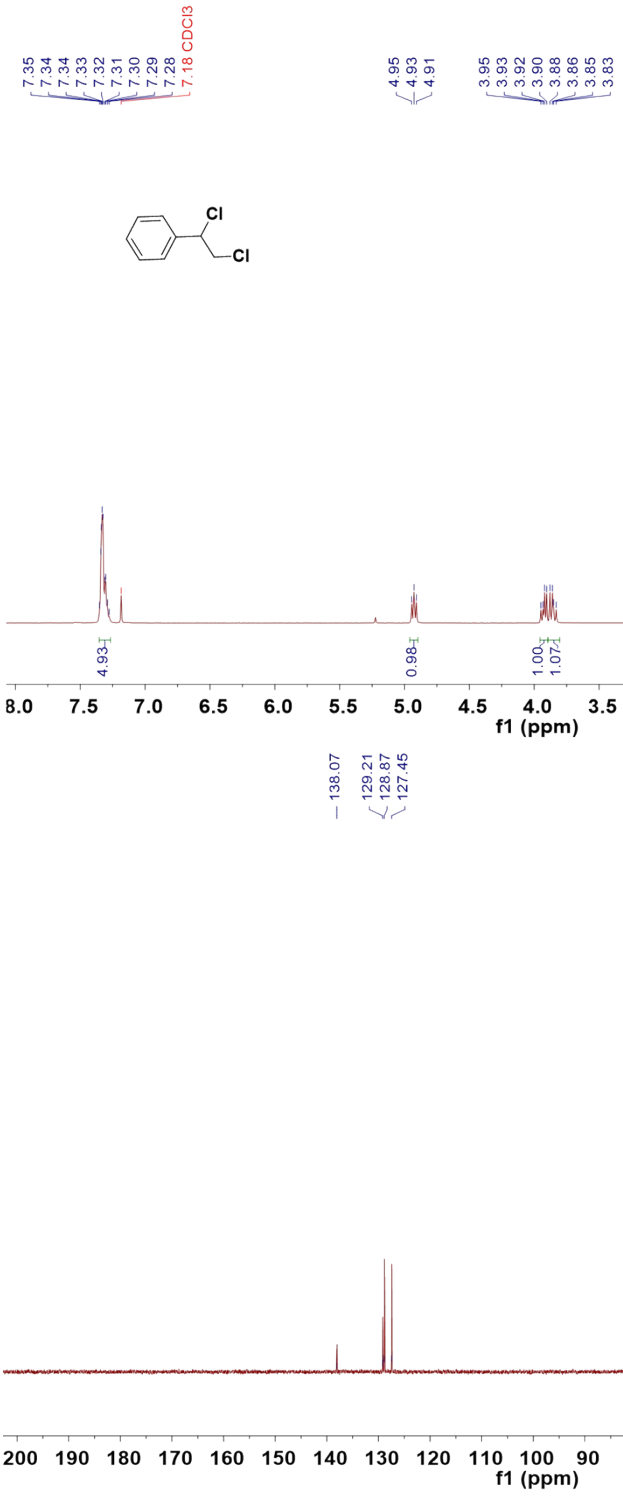

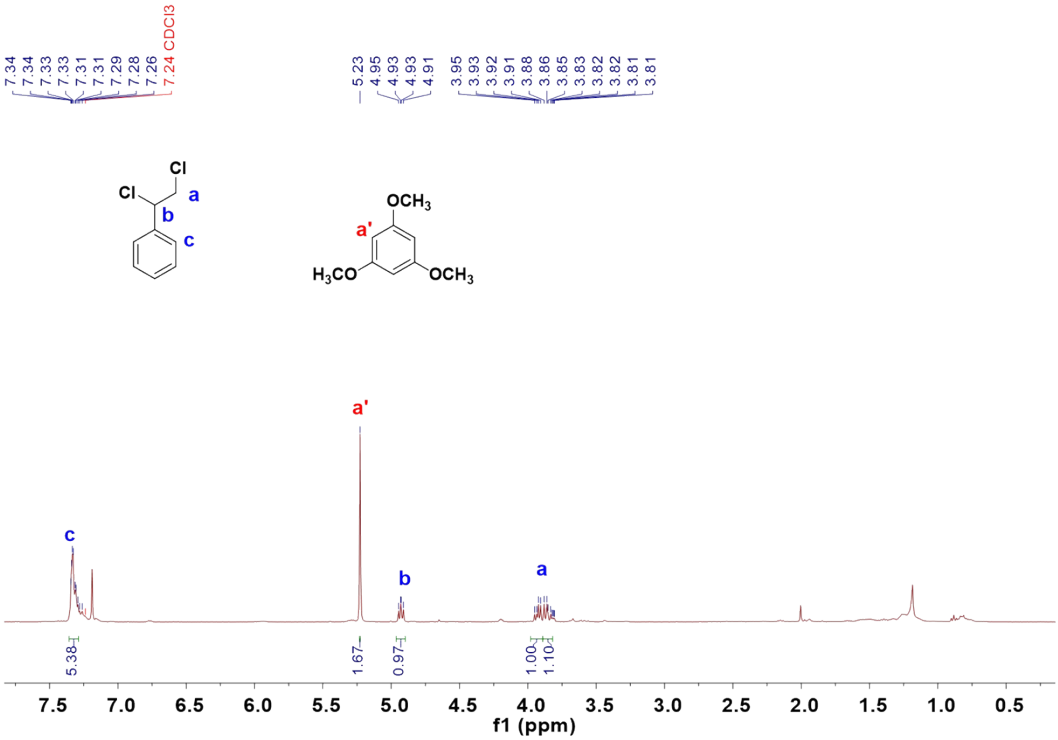

^{1}H NMR spectrum of the products of PEC vicinal dichlorination of 1,2-dichlorostyrene (compound **1**) in 0.1 M Net_4BF_4 electrolyte (2% H_2O, 98% CH_3CN (V%)) with 0.1 mmol styrene, 4 eq HCl and 10 µmol $MnCl_2$ at 1.0 V vs. Ag/AgCl under AM 1.5G, 100 mW/cm^2 irradiation for 2 h.

1-(1,2-dichloroethyl)-4-fluorobenzene

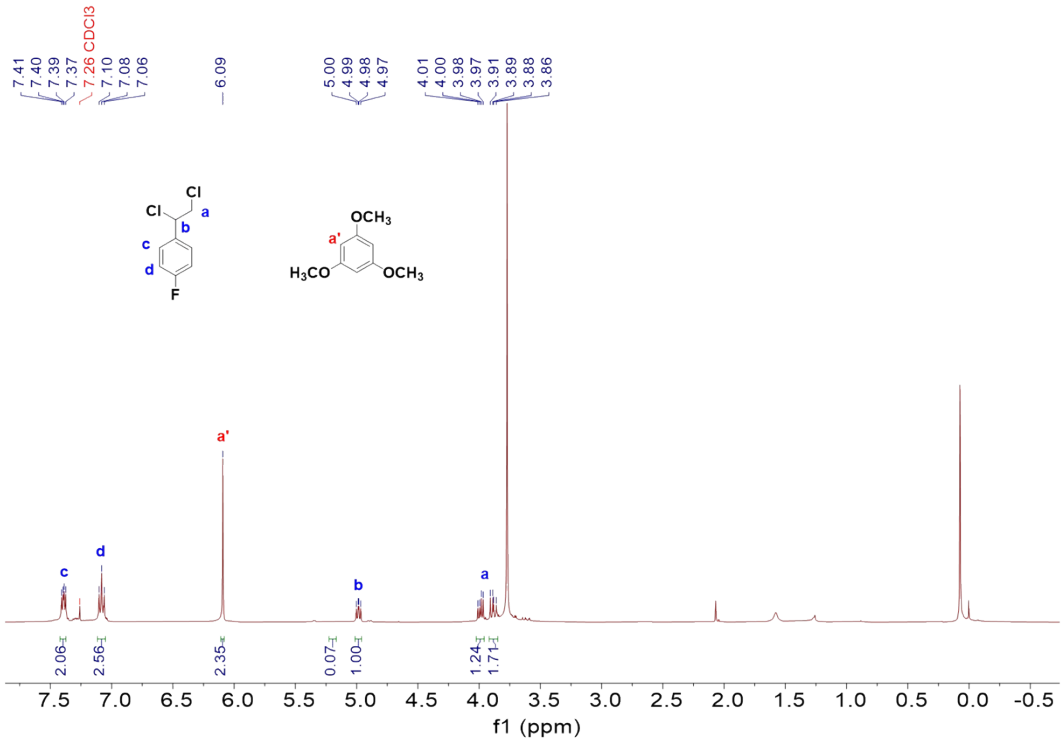

^{1}H NMR spectrum of the products of PEC vicinal dichlorination of 1-(1,2-dichloroethyl)-4-fluorobenzene (compound **2**) in 0.1 M Net_4BF_4 electrolyte (2% H_2O, 98% CH_3CN (V%)) with 0.1 mmol 4-fluorostyrene, 4 eq HCl and 10 µmol $MnCl_2$ at 1.0 V vs. Ag/AgCl under AM 1.5G, 100 mW/cm^2 irradiation for 4 h.

1-chloro-4-(1,2-dichloroethyl) benzene

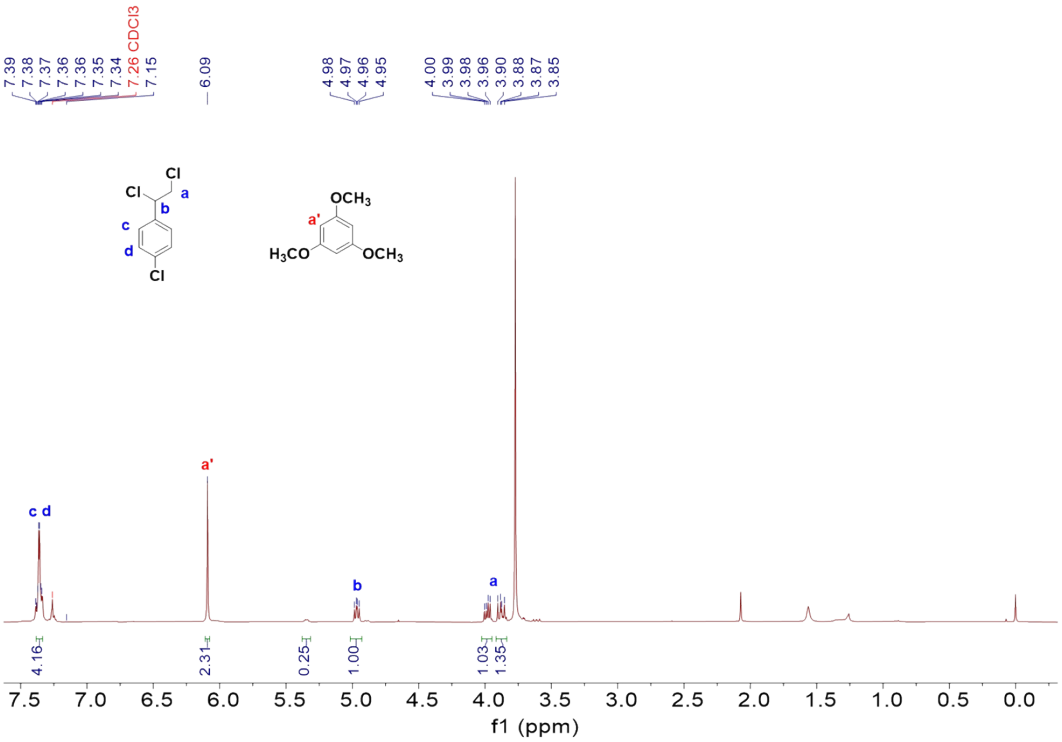

^{1}H NMR spectrum of the products of PEC vicinal dichlorination of 1-chloro-4-(1,2-dichloroethyl) benzene (compound **3**) in 0.1 M Net_4BF_4 electrolyte (2% H_2O, 98% CH_3CN (V%)) with 0.1 mmol 1-chloro-4-vinylbenzene, 4 eq HCl and 10 μmol $MnCl_2$ at 1.0 V vs. Ag/AgCl under AM 1.5G, 100 mW/cm^2 irradiation for 4 h.

1-bromo-4-(1,2-dichloroethyl) benzene

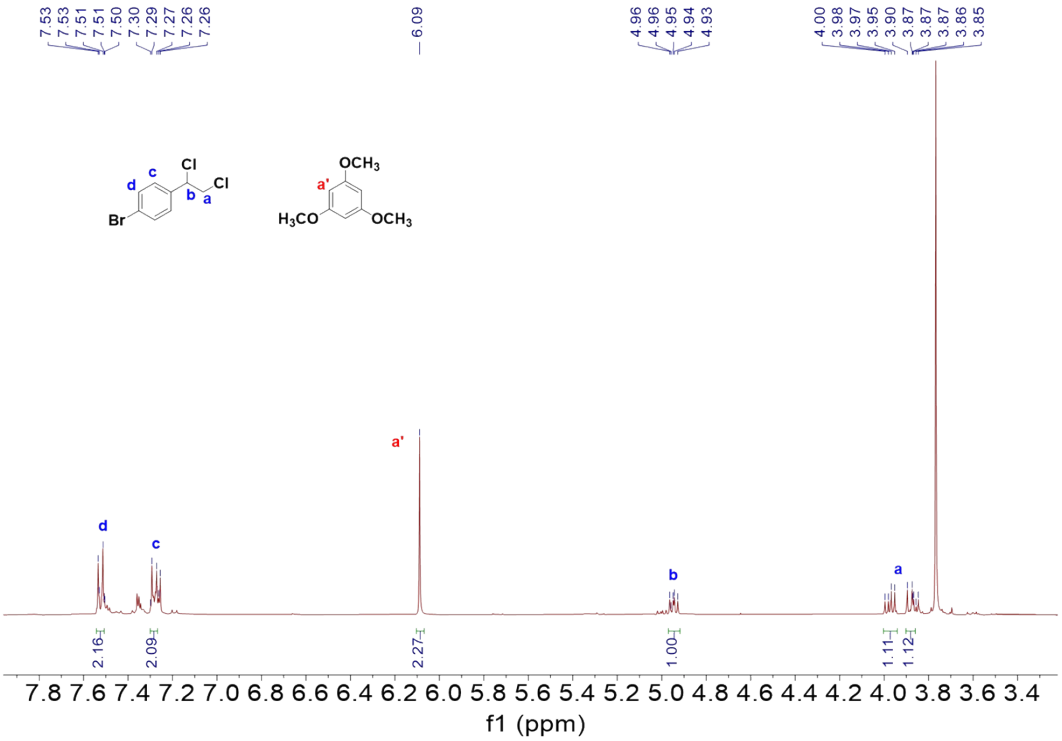

^{1}H NMR spectrum of the products of PEC vicinal dichlorination of 1-bromo-4-(1,2-dichloroethyl) benzene (compound **4**) in 0.1 M Net_4BF_4 electrolyte (2% H_2O, 98% CH_3CN (V%)) with 0.1 mmol 1-bromo-4-ethenyl-benzene, 4 eq HCl and 10 μmol $MnCl_2$ at 1.0 V vs. Ag/AgCl under AM 1.5G, 100 mW/cm^2 irradiation for 4 h.

1-(1,2-dichloroethyl)-4-methylbenzene

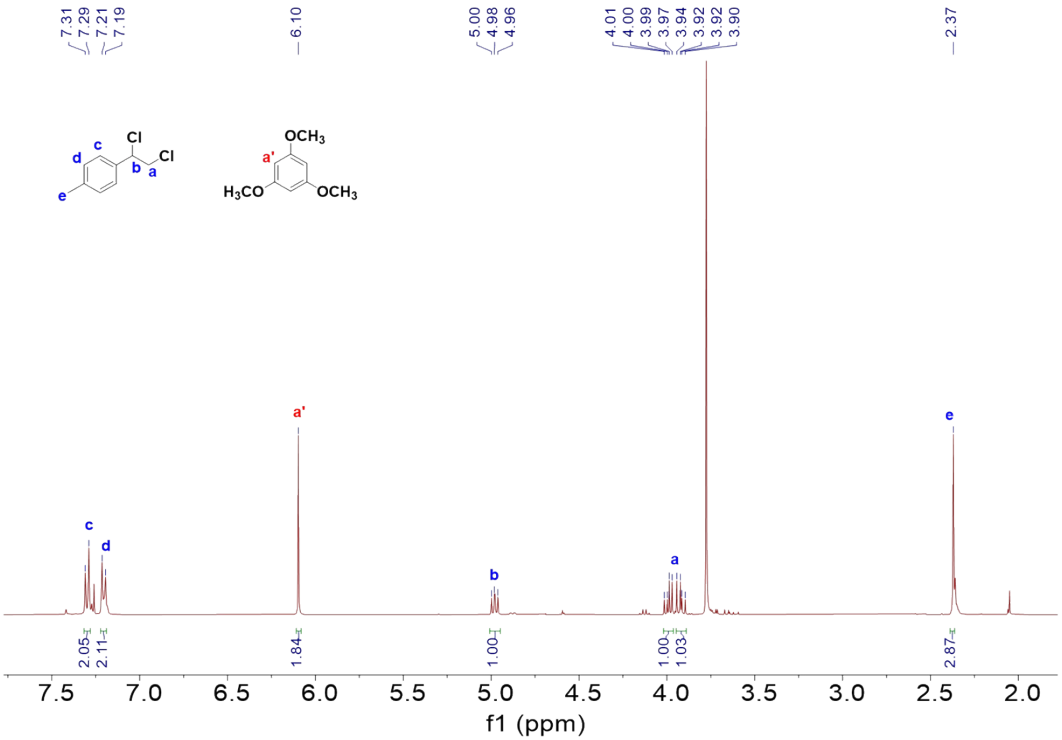

^{1}H NMR spectrum of the products of PEC vicinal dichlorination of 1-(1,2-dichloroethyl)-4-methylbenzene (compound **5**) in 0.1 M Net_4BF_4 electrolyte (2% H_2O, 98% CH_3CN (V%)) with 0.1 mmol 1-ethenyl-4-methylbenzene, 4 eq HCl and 10 µmol $MnCl_2$ at 1.0 V vs. Ag/AgCl under AM 1.5G, 100 mW/cm^2 irradiation for 4 h.

4-(1,2-dichloroethyl) benzonitrile

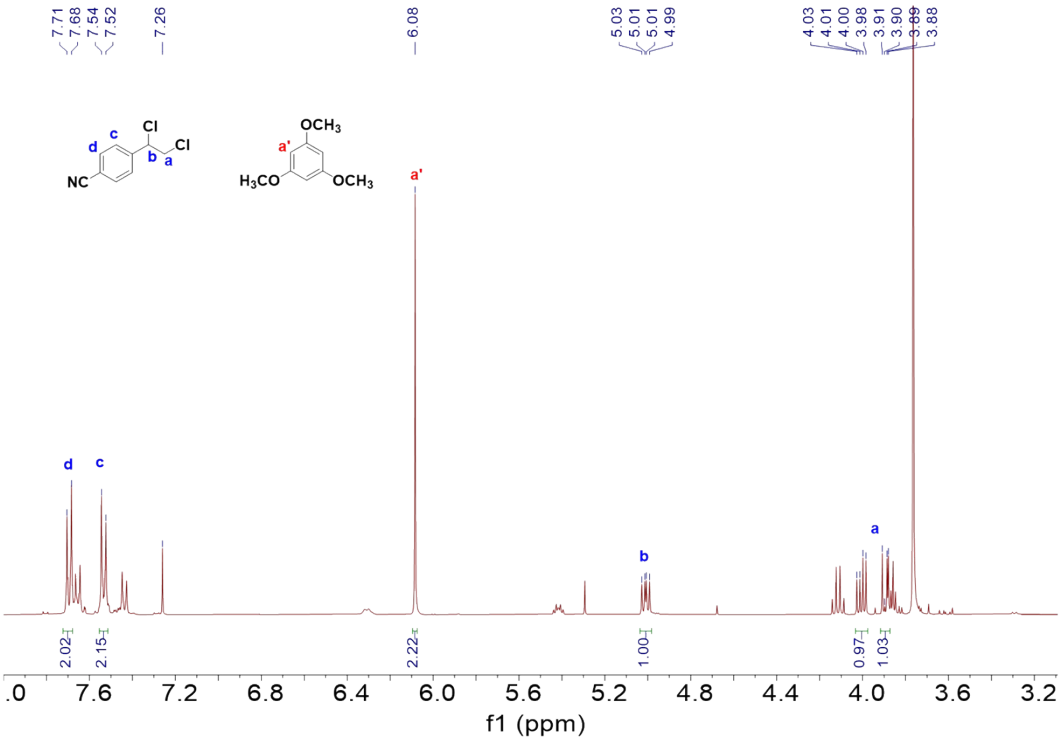

^{1}H NMR spectrum of the products of PEC vicinal dichlorination of 4-(1,2-dichloroethyl) benzonitrile (compound **6**) in 0.1 M Net_4BF_4 electrolyte (2% H_2O, 98% CH_3CN (V%)) with 0.1 mmol 4-ethenylbenzonitrile, 4 eq HCl and 10 µmol $MnCl_2$ at 1.0 V vs. Ag/AgCl under AM 1.5G, 100 mW/cm^2 irradiation for 4 h.

bromo-3-(1,2-dichloroethyl) benzene

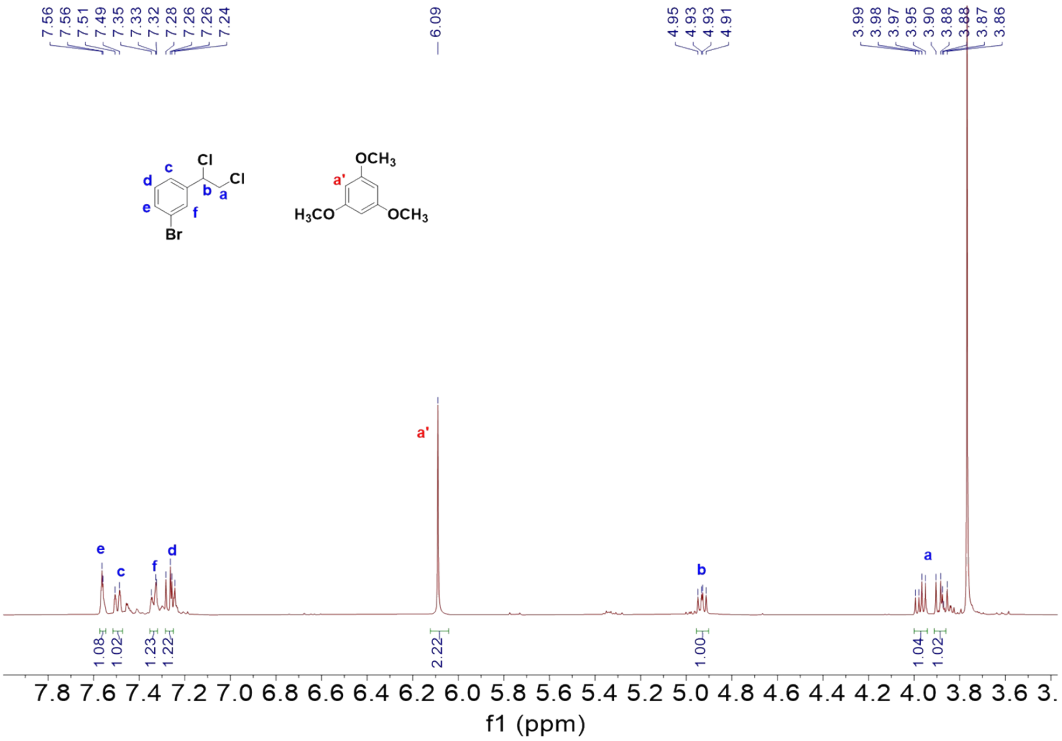

^{1}H NMR spectrum of the products of PEC vicinal dichlorination of bromo-3-(1,2-dichloroethyl) benzene (compound **7**) in 0.1 M Net_4BF_4 electrolyte (2% H_2O, 98% CH_3CN (V%)) with 0.1 mmol 3-bromostyrene, 4 eq HCl and 10 µmol $MnCl_2$ at 1.0 V vs. Ag/AgCl under AM 1.5G, 100 mW/cm^2 irradiation for 4 h.

2-phenyl-1-propene

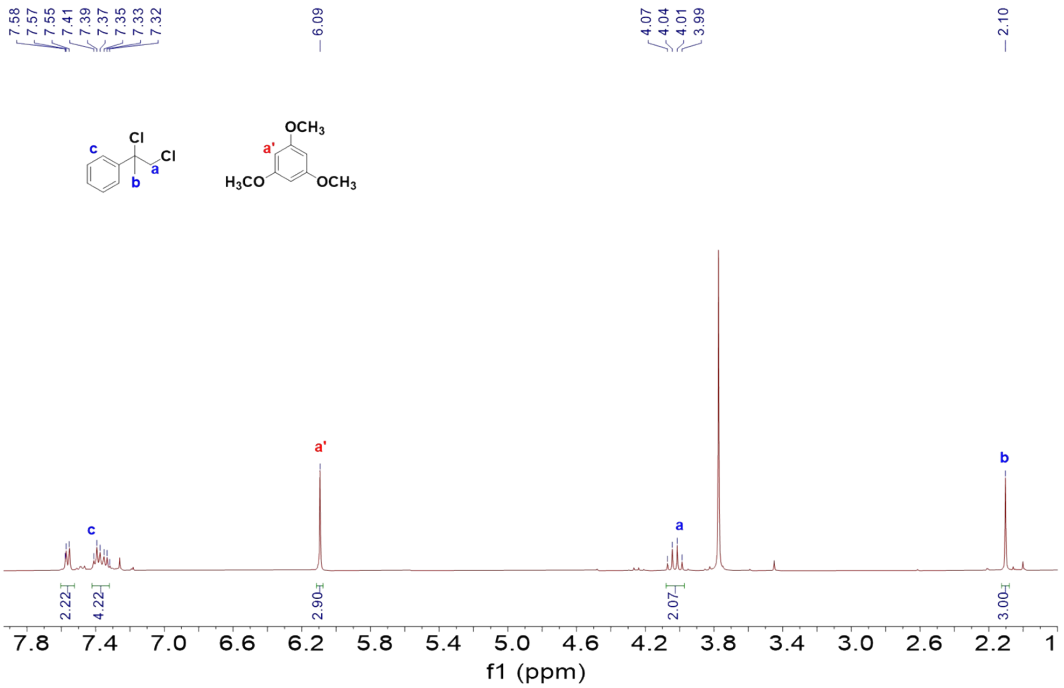

^{1}H NMR spectrum of the products of PEC vicinal dichlorination of 2-phenyl-1-propene (compound **8**) in 0.1 M Net_4BF_4 electrolyte (2% H_2O, 98% CH_3CN (V%)) with 0.1 mmol isopropenylbenzene, 4 eq HCl and 10 μmol $MnCl_2$ at 1.0 V vs. Ag/AgCl under AM 1.5G, 100 mW/cm^2 irradiation for 4 h.

1,2-dichloro-2,3-dihydro-1H-indene

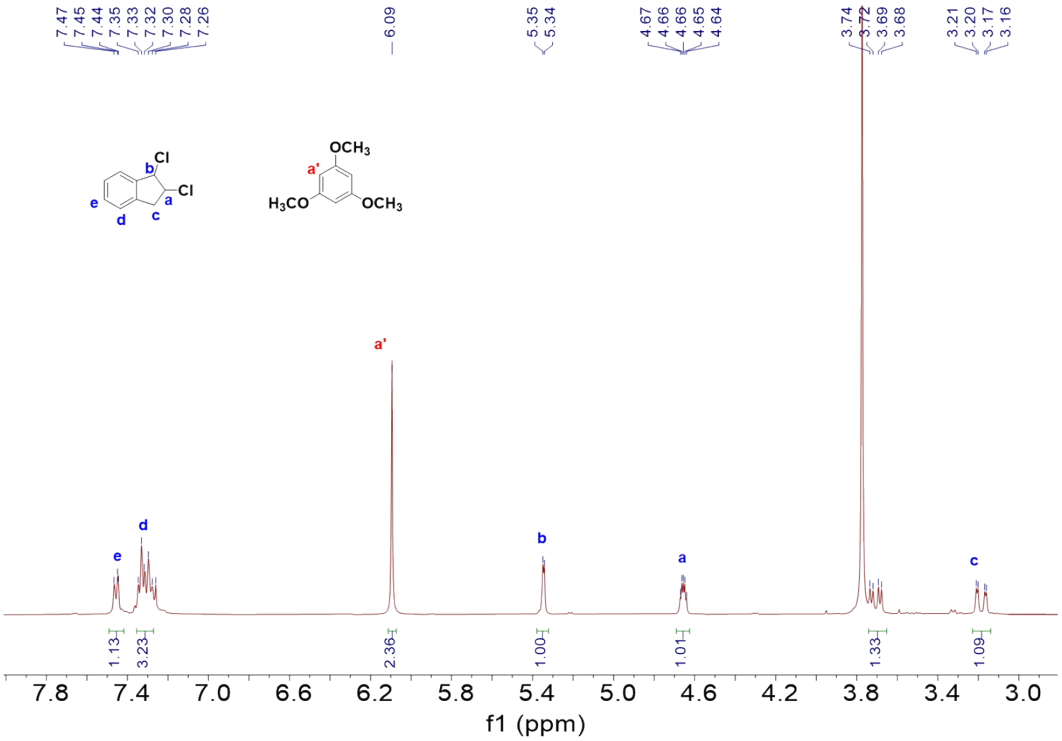

^{1}H NMR spectrum of the products of PEC vicinal dichlorination of 1,2-dichloro-2,3-dihydro-1H-indene (compound **9**) in 0.1 M Net_4BF_4 electrolyte (2% H_2O, 98% CH_3CN (V%)) with 0.1 mmol 1-indene, 4 eq HCl and 10 µmol $MnCl_2$ at 1.0 V vs. Ag/AgCl under AM 1.5G, 100 mW/cm^2 irradiation for 4 h.

((1R)-1,2-dichloropropyl) benzene

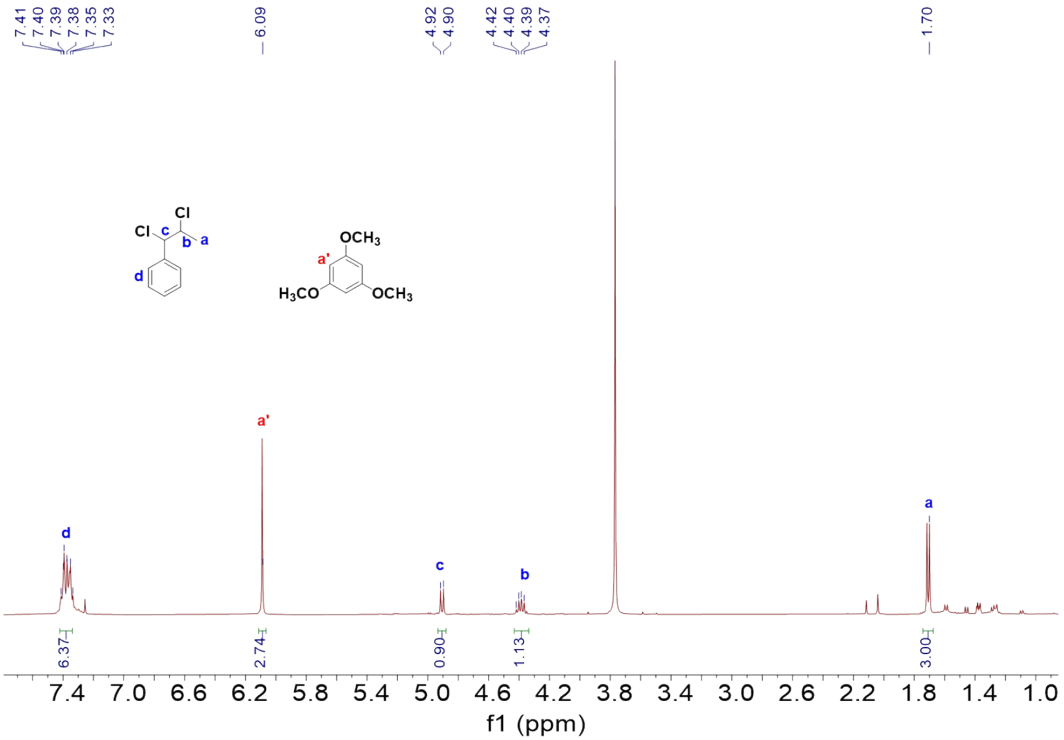

^{1}H NMR spectrum of the products of PEC vicinal dichlorination of ((1R)-1,2-dichloropropyl) benzene (compound **10**) in 0.1 M Net_4BF_4 electrolyte (2% H_2O, 98% CH_3CN (V%)) with 0.1 mmol 1-propenylbenzene, 4 eq HCl and 10 μmol $MnCl_2$ at 1.0 V vs. Ag/AgCl under AM 1.5G, 100 mW/cm^2 irradiation for 4 h.

(3,4-dichlorobutyl) benzene

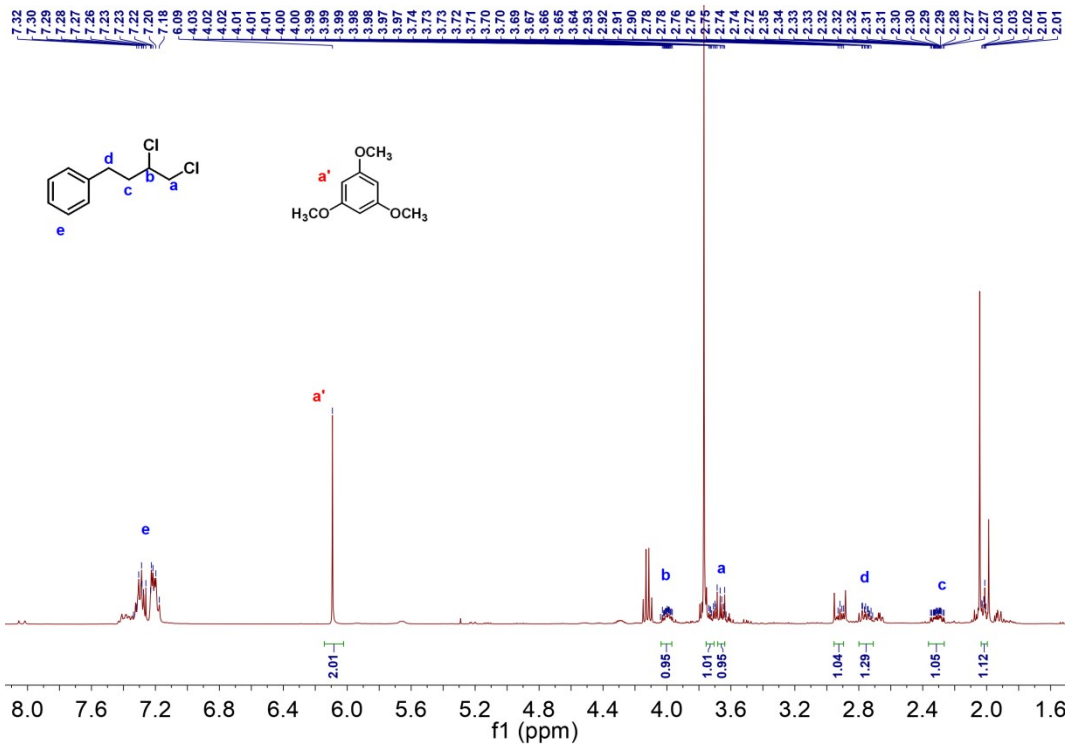

^{1}H NMR spectrum of the products of PEC vicinal dichlorination of (3,4-dichlorobutyl) benzene (compound **11**) in 0.1 M Net_4BF_4 electrolyte (2% H_2O, 98% CH_3CN (V%)) with 0.1 mmol 3-butenylbenzene, 4 eq HCl and 10 μmol $MnCl_2$ at 1.0 V vs. Ag/AgCl under AM 1.5G, 100 mW/cm^2 irradiation for 4 h.

2-(1,2-dichloroethyl) naphthalene

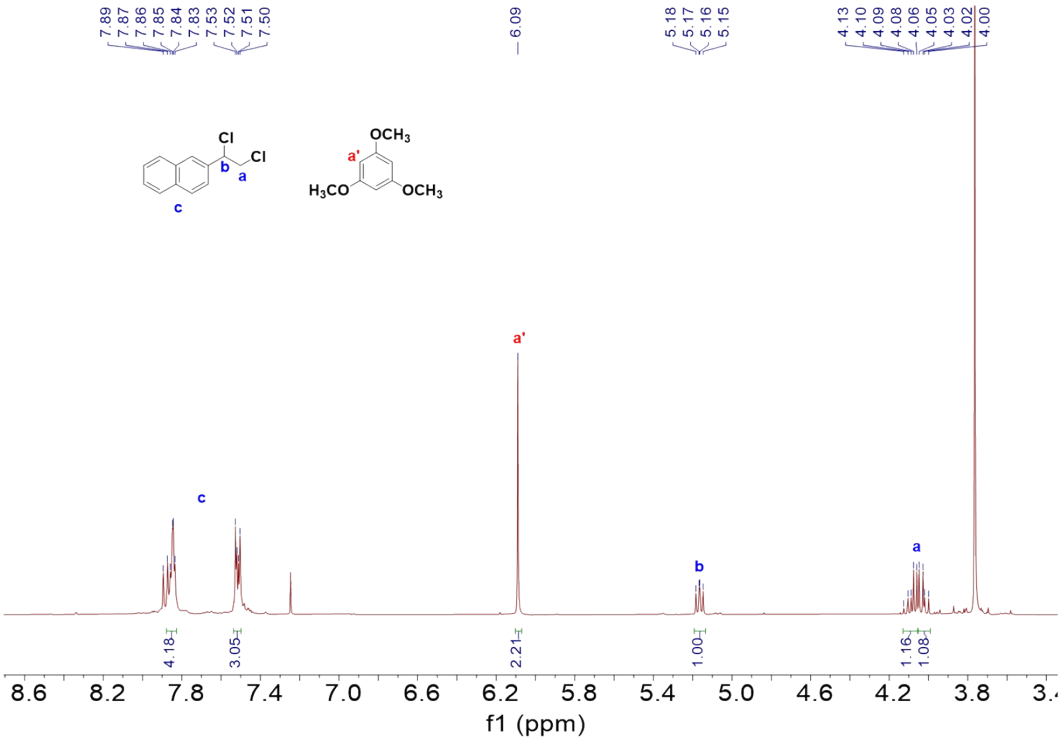

^{1}H NMR spectrum of the products of PEC vicinal dichlorination of 2-(1,2-dichloroethyl) naphthalene (compound **12**) in 0.1 M Net_4BF_4 electrolyte (2% H_2O, 98% CH_3CN (V%)) with 0.1 mmol 2-vinylnaphthalene, 4 eq HCl and 10 μmol $MnCl_2$ at 1.0 V vs. Ag/AgCl under AM 1.5G, 100 mW/cm^2 irradiation for 4 h.

4-(1,2-dichloroethyl)-1,1'-biphenyl

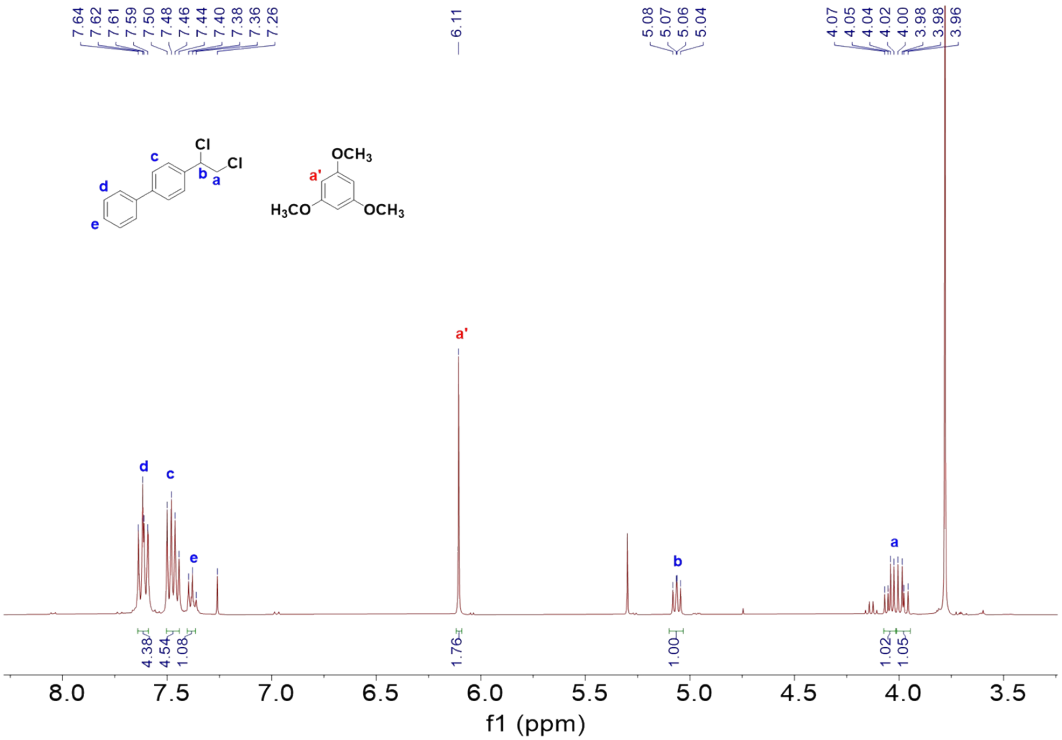

^{1}H NMR spectrum of the products of PEC vicinal dichlorination of 4-(1,2-dichloroethyl)-1,1'-biphenyl (compound **13**) in 0.1 M Net_4BF_4 electrolyte (2% H_2O, 98% CH_3CN (V%)) with 0.1 mmol 4-vinyl-1,1'-biphenyl, 4 eq HCl and 10 μmol $MnCl_2$ at 1.0 V vs. Ag/AgCl under AM 1.5G, 100 mW/cm^2 irradiation for 4 h.

2,3-dichloro-3-methylbutyl benzoate

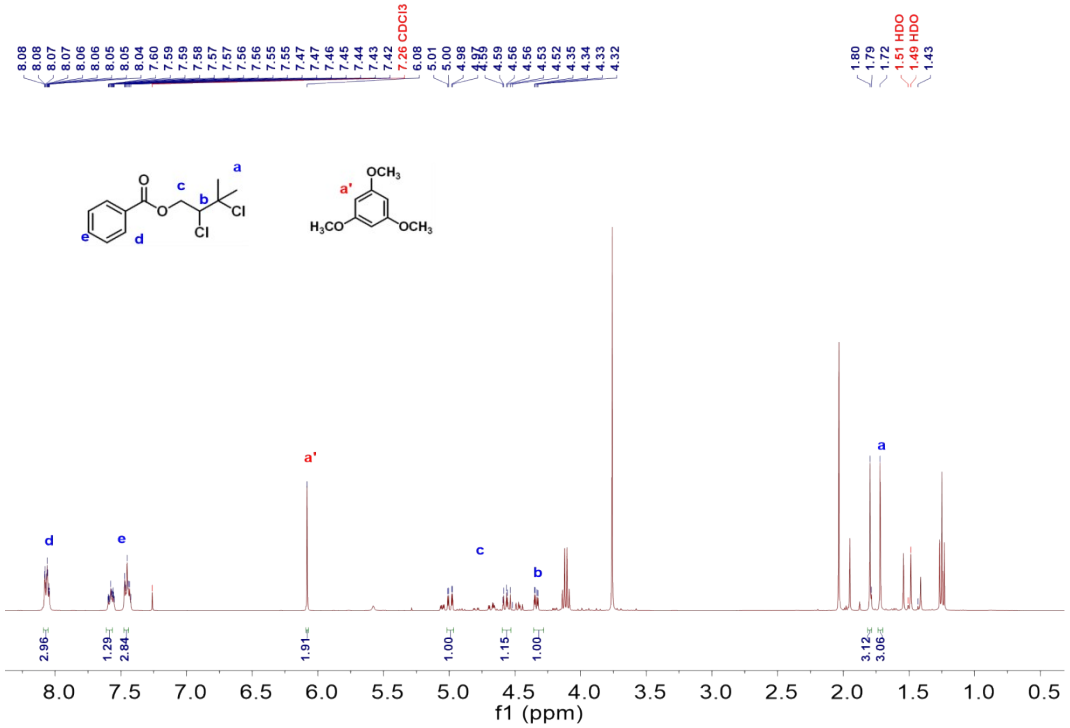

^{1}H NMR spectrum of the products of PEC vicinal dichlorination of 2,3-dichloro-3-methylbutyl benzoate (compound **14**) in 0.1 M Net_4BF_4 electrolyte (2% H_2O, 98% CH_3CN (V%)) with 0.1 mmol 3-methyl-2-butenyl benzoate, 4 eq HCl and 10 µmol $MnCl_2$ at 1.0 V vs. Ag/AgCl under AM 1.5G, 100 mW/cm^2 irradiation for 6 h.

benzyl-(1,2-dichloro-ethyl)-ether

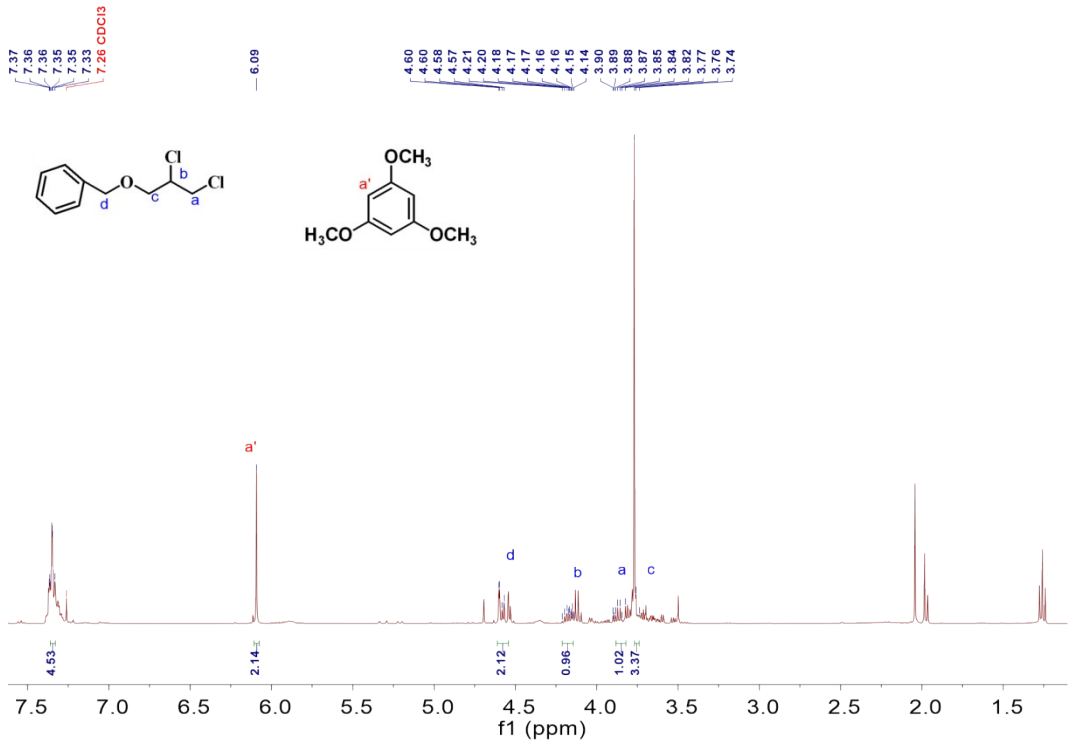

1H NMR spectrum of the products of PEC vicinal dichlorination of benzyl-(1,2-dichloro-ethyl)-ether (compound **15**) in 0.1 M Net_4BF_4 electrolyte (2% H_2O, 98% CH_3CN (V%)) with 0.1 mmol benzyl vinyl ether, 4 eq HCl and 10 µmol $MnCl_2$ at 1.0 V vs. Ag/AgCl under AM 1.5G, 100 mW/cm^2 irradiation for 4 h.

10,11-dichloroundecan-1-ol

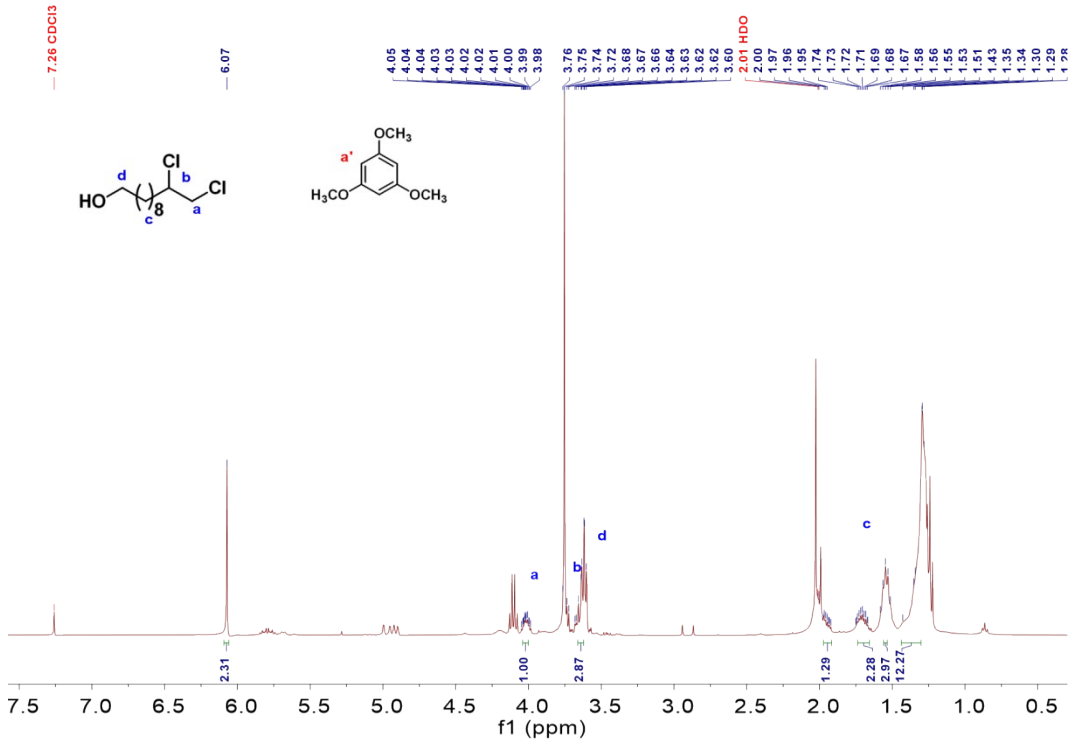

^{1}H NMR spectrum of the products of PEC vicinal dichlorination of 10,11-dichloroundecan-1-ol (compound **16**) in 0.1 M Net_4BF_4 electrolyte (2% H_2O, 98% CH_3CN (V%)) with 0.1 mmol 10-undecen-1-ol, 4 eq HCl and 10 μmol $MnCl_2$ at 1.0 V vs. Ag/AgCl under AM 1.5G, 100 mW/cm^2 irradiation for 4 h.

11-bromo-1,2-dichloroundecane

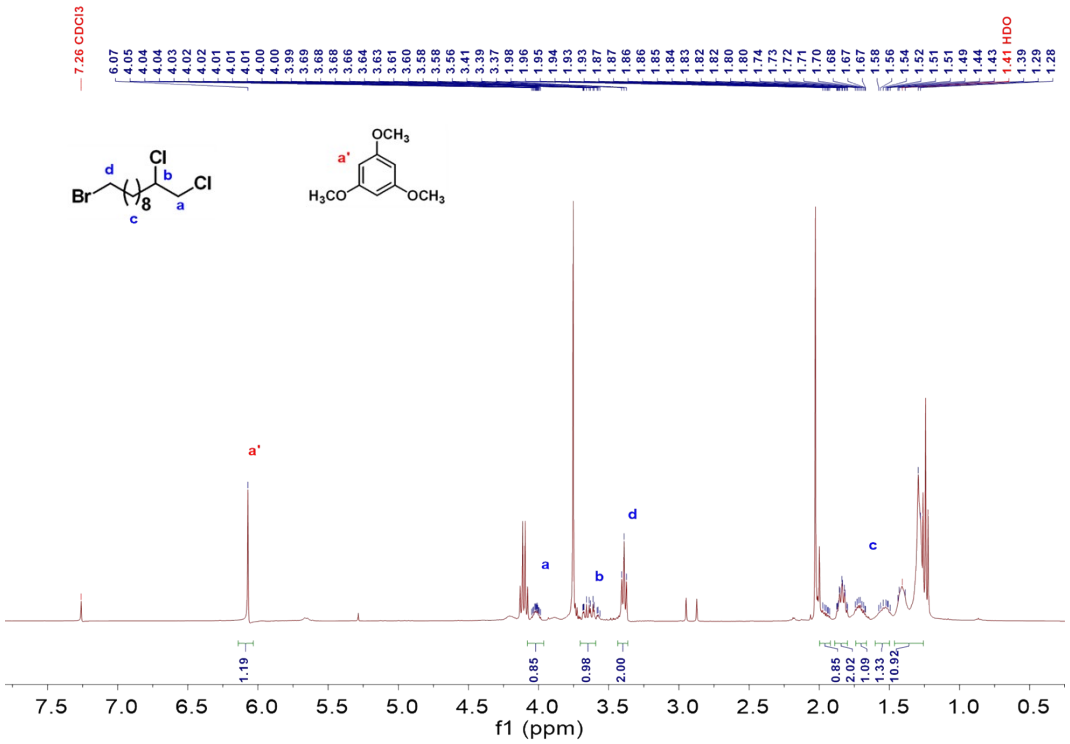

^{1}H NMR spectrum of the products of PEC vicinal dichlorination of 11-bromo-1,2-dichloroundecane (compound **17**) in 0.1 M Net_4BF_4 electrolyte (2% H_2O, 98% CH_3CN (V%)) with 0.1 mmol 1-undecen-11-ylbromide, 4 eq HCl and 10 μmol $MnCl_2$ at 1.0 V vs. Ag/AgCl under AM 1.5G, 100 mW/cm^2 irradiation for 4 h.

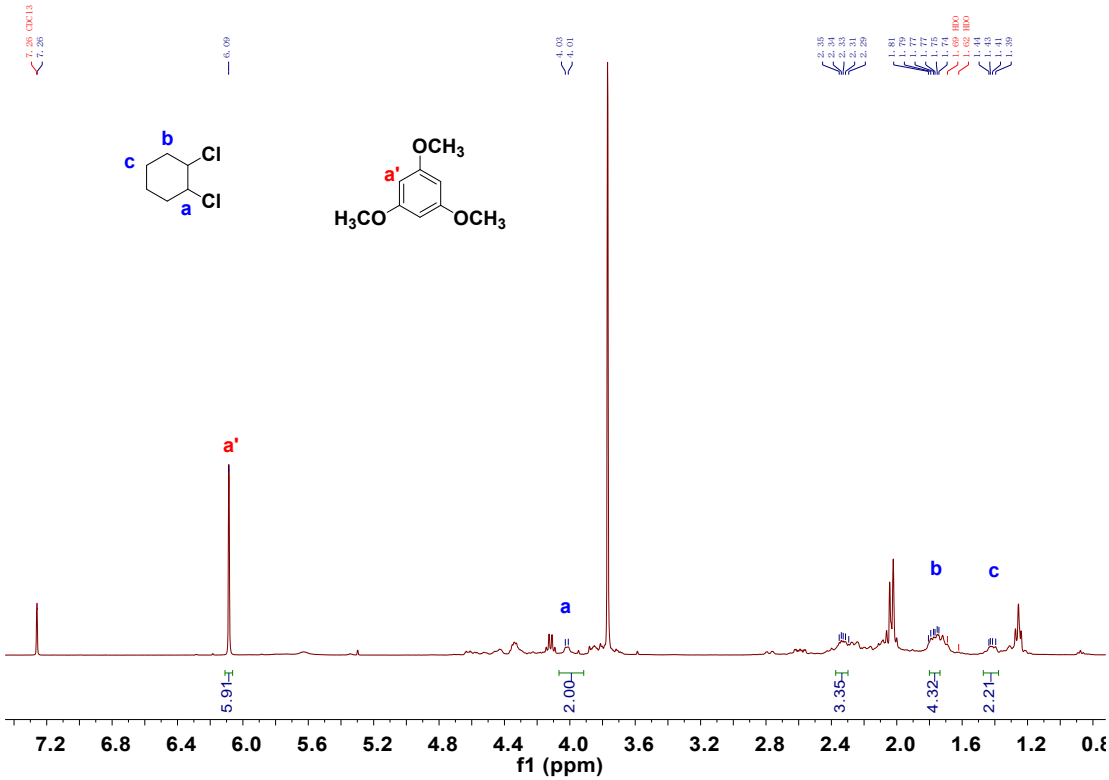

^{1}H NMR spectrum of the products of PEC vicinal dichlorination of dichlorocyclohexane (compound **18**) in 0.1 M Net_4BF_4 electrolyte (2% H_2O, 98% CH_3CN (V%)) with 0.1 mmol cyclohexene, 4 eq HCl and 10 μmol $MnCl_2$ at 1.0 V vs. Ag/AgCl under AM 1.5G, 100 mW/cm^2 irradiation for 7 h.

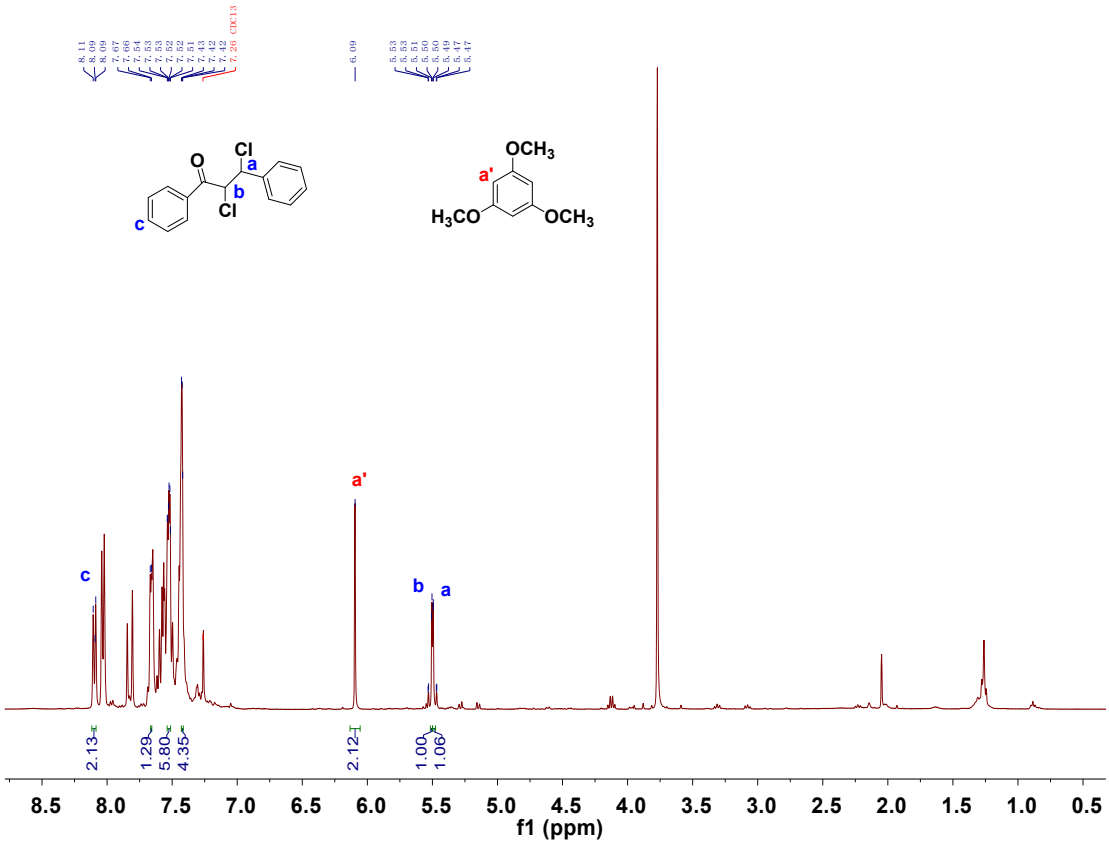

^{1}H NMR spectrum of the products of PEC vicinal dichlorination of 1-Propanone,2,3-dichloro-1,3-diphenyl (compound **19**) in 0.1 M Net_4BF_4 electrolyte (2% H_2O, 98% CH_3CN (V%)) with 0.1 mmol chalcone, 4 eq HCl and 10 µmol $MnCl_2$ at 1.0 V vs. Ag/AgCl under AM 1.5G, 100 mW/cm^2 irradiation for 7 h.

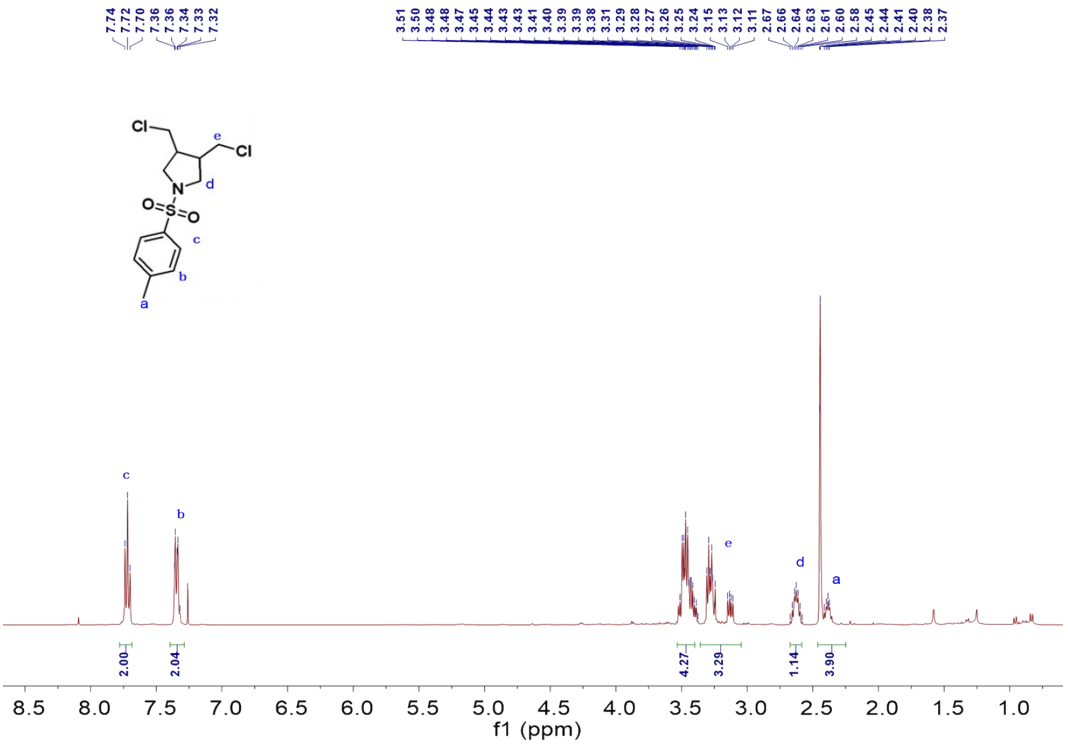

^{1}H NMR spectrum of the pure cyclic product of PEC vicinal dichlorination of 3,4-bis(chloromethyl)-1-tosylpyrrolidine (compound **20**) in 0.1 M Net_4BF_4 electrolyte (2% H_2O, 98% CH_3CN (V%)) with 0.1 mmol N, N-diallyltosylamide at 1.0 V vs. Ag/AgCl under AM 1.5G, 100 mW/cm^2 irradiation for 2 h.

4. Notes and references

1. J. Xue, L. Wu, C. Deng, D. Tang, S. Wang, H. Ji, C. Chen, Y. Zhang and J. Zhao, *ACS Applied Nano Materials*, 2022, **5**, 11342-11351.
2. X. Shi, Q. Wu and C. Cui, *ACS Catalysis*, 2023, **13**, 1470-1476.
3. L. Wu, D. Tang, J. Xue, S. Wang, H. Ji, C. Chen, Y. Zhang and J. Zhao, *Science China Chemistry*, 2023, **66**, 896–903.
4. D. Tang, L. Wu, L. Li, N. Fu, C. Chen, Y. Zhang and J. Zhao, *Chemical Science*, 2024, **15**, 3018-3027.
5. H. Li, C. Lin, Y. Yang, C. Dong, Y. Min, X. Shi, L. Wang, S. Lu and K. Zhang, *Angewandte Chemie International Edition*, 2022, **62**, e202210804
6. Q. Mi, A. Zhanaidarova, B. S. Brunschwig, H. B. Gray and N. S. Lewis, *Energy & Environmental Science*, 2012, **5**, 5694.
7. J. Ma, K. Mao, J. Low, Z. Wang, D. Xi, W. Zhang, H. Ju, Z. Qi, R. Long, X. Wu, L. Song and Y. Xiong, *Angewandte Chemie International Edition*, 2021, **60**, 9357-9361.
8. Z. Li, L. Luo, M. Li, W. Chen, Y. Liu, J. Yang, S.-M. Xu, H. Zhou, L. Ma, M. Xu, X. Kong and H. Duan, *Nature Communications*, 2021, **12**, 6698.
9. Z. Wu, P. Yang, Q. Li, W. Xiao, Z. Li, G. Xu, F. Liu, B. Jia, T. Ma, S. Feng and L. Wang, *Angewandte Chemie International Edition*, 2023, **62**, e202300406.
10. M. Mao, Y. Qi, K. Lu, Q. Chen, X. Xie, X. Li, Z. Lin, L. Chai and W. Liu, *Environmental Science & Technology*, 2024, **58**, 14013-14021.
11. Y. Huang, Z. Zhang and D. Xing, *ACS Applied Nano Materials*, 2022, **5**, 4609-4614.
12. G. Wang, H. Wang, Y. Ling, Y. Tang, X. Yang, R. C. Fitzmorris, C. Wang, J. Z. Zhang and Y. Li, *Nano Letters*, 2011, **11**, 3026-3033.
13. H. Yun, J. Li, H.-B. Chen and C.-J. Lin, *Electrochimica Acta*, 2007, **52**, 6679-6685.
14. C. Ma, C. Yang, H. Zhuo, C. Chen, K. Lu, F. Wang, Z. Shi, H. Xiao, M. Song and G. Jiang, *Journal of the American Chemical Society*, 2023, **145**, 10890-10898.
15. D. P. Jaihindh, P. Anand, R.-S. Chen, W.-Y. Yu, M.-S. Wong and Y.-P. Fu, *Journal of Environmental Chemical Engineering*, 2023, **11**, 109852.
16. D. Xu, T. Xia, H. Xu, W. Fan and W. Shi, *Chemical Engineering Journal*, 2020, **392**, 124838.
17. S. Niu, X.-P. Kong, S. Li, Y. Zhang, J. Wu, W. Zhao and P. Xu, *Applied Catalysis B: Environmental*, 2021, **297**, 120442.